Chinese Chemical Letters 34 (2023) 108050

Contents lists available at ScienceDirect

Chinese Chemical Letters

journal homepage: www.elsevier.com/locate/cclet

Preparation and characterization of M_1-N_x-C_y based single atom catalysts for environmental applications

Xinjiang Hu[a,b,*], Daixi Zhou[a], Hui Wang[a], Wenlong Zhang[b,c], Haoxiang Zhong[a], Yongsheng Chen[b,**]

[a] College of Environmental Science and Engineering, Central South University of Forestry and Technology, Changsha 410004, China
[b] School of Civil and Environmental Engineering, Georgia Institute of Technology, Atlanta, GA 30332, United States
[c] Georgia Tech Shenzhen Institute, Tianjin University, Shenzhen 518067, China

ARTICLE INFO

Article history:
Received 31 August 2022
Revised 18 November 2022
Accepted 6 December 2022
Available online 8 December 2022

Keywords:
Single atom catalysts
Photocatalysis
Electrocatalysis
Environmental applications

ABSTRACT

Single atom catalysts (SACs) have become the frontier research fields in catalysis. The M_1-N_x-C_y based SACs, wherein single metal atoms (M_1) are stabilized by N-doped carbonaceous materials, have provided new opportunities for catalysis due to their high reactivity, maximized atomic utilization, and high selectivity. In this review, the fabrication methods of M_1-N_x-C_y based SACs *via* support anchoring strategy and coordination design strategy are summarized to help the readers understand the interaction mechanism of single atoms and support. Then, characterization technologies for identifying single metal atoms are presented. Besides, the environmental applications including management of harmful gases, water purification are discussed. Finally, future opportunities and challenges for preparation strategies, mechanisms and applications are concluded. We conclude this review by emphasizing the fact that M_1-N_x-C_y based SACs has the potential to become an important candidate for solving current and future environmental pollution problems.

1. Introduction

With increasing population, accelerating urbanization, and rising living standards, the energy and environmental issues have attracted more global attention than ever [1]. The development of low-cost, high-efficiency, clean and sustainable energy conversion and storage systems has become a top priority [2]. Additionally, the ecological imbalances due to environmental pollution in air and water need to be resolved as soon as possible. Catalysis plays a critical role in solving environment-related problems [1]. The efficiency of a catalytic process strongly depends on the structure and performance of the catalyst. Consequently, scientists continuously seek to develop low cost catalysts with highly efficient and selective performance [3].

According to the phases of reaction systems, catalysis can be classified as homogeneous and heterogeneous. Homogeneous catalysts often have uniform active centers with high activity and selectivity [4]. However, homogeneous catalysts are not easily recycled because they are difficult to separate from raw materials and products [5]. In contrast, heterogeneous catalysts are usually relatively stable in the reaction system and easy to separate, but their active sites may be non-uniform with low efficiency and selectivity [4,5]. Therefore, both types of the catalysts have their own merits and limits. One possible method to overcome the drawbacks of the homogeneous catalysts is anchoring molecular metal complexes to an insoluble support [4–6]. However, this type of catalyst has not been widely used in industry [6]. Meanwhile, the activity and selectivity of heterogeneous catalysts have a significant correlation with their size and shape [7]. Therefore, reducing the particle size of the catalyst is one of the most effective ways to improve its performance [8]. We can see that there is a gap between homogeneous catalysts and heterogeneous catalysts [9]. Then, can we build a bridge between them for incorporating their advantageous features?

For the metal-based heterogeneous catalysts, downsizing the metal particles on solid supports to single atoms can generate the single atom catalysts (SACs) [7], which may be the most suitable candidate for bridging the gap between homogeneous and heterogeneous catalysts (Fig. 1) [10,11]. The SACs exhibit robust activity owing to the 100% metal atom utilization [12–16], and it also pro-

* Corresponding author at: College of Environmental Science and Engineering, Central South University of Forestry and Technology, Changsha 410004, China.
** Corresponding author.
E-mail addresses: xjhu@csuft.edu.cn (X. Hu), yongsheng.chen@ce.gatech.edu (Y. Chen).

https://doi.org/10.1016/j.cclet.2022.108050
1001-8417/

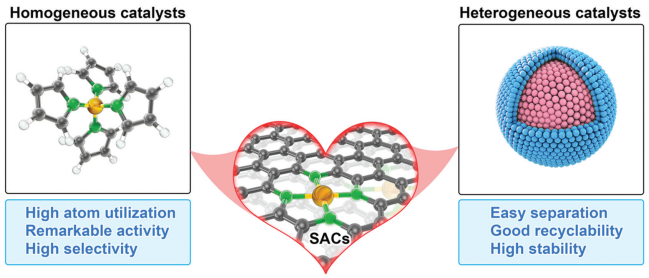

Fig. 1. Bridging the gap between homogeneous and heterogeneous catalysts by SACs.

vide a good strategy to prepare cost-effective earth-scarce metal catalysts [10]. In fact, the single metal atoms on SACs are not really isolated, but they are stabilized by covalent coordination or ionic interactions with neighboring atoms on the support, which indicates that the structure and composition of the support play an important role in the electronic properties and catalytic activity of SACs [6,17,18]. Many different types of supports such as metal compound [7,14,19], organic ligand modified materials [10], alloy [20,21], and N-doped carbonaceous materials [22,23], have been developed for stabilizing the single metal atoms. Among of which, the N-doped carbonaceous materials have attracted great attention because carbon and nitrogen atoms can easily form stable bond and coordination structures with single metal atoms to obtain the cost-effective, active, and durable M_1-N_x-C_y based SACs [3,22].

Recently, several reviews based on the use of SACs for energy applications were published [24,25]. In Shang's article, recent single-atom catalysis in advanced oxidation processes for environmental remediation is summarized [26]. Nevertheless, to the best of our knowledge, there is currently no review focused only on M_1-N_x-C_y based SACs, and their environmental applications. Besides, there is still a lack of review articles that classify the preparation methods of M_1-N_x-C_y based SACs according to the interaction mechanism of single atoms and supports (support anchoring strategy and coordination design strategy). Moreover, no review analyzed the density functional theory (DFT) calculations of M_1-N_x-C_y based SACs based on optimal catalyst design, catalytic activity calculation, and catalytic mechanism simulation. Herein, we first review the preparation methods of M_1-N_x-C_y based SACs in two aspects: support anchoring strategy and coordination design strategy. Then, we present the advanced characterization technology for identifying of single metal atoms in the M_1-N_x-C_y based SACs from three perspectives: microscopic techniques, spectroscopic techniques, and DFT calculations. We also separately highlight the recent progresses on the applications of M_1-N_x-C_y based SACs in harmful gases management (conversion of CO, NO, and H_2S) and water purification (Fenton-like catalysis, photocatalytic degradation, and electrochemical filtration) are summarized. Moreover, the opportunities and challenges for the development of this field are discussed.

2. Preparation of M_1-N_x-C_y based SACs

Single metal atoms usually have high surface energy, which promotes their aggregation during the synthetic and catalytic processes [27]. Therefore, in order to obtain highly active M_1-N_x-C_y based SACs, there are two challenges regarding preparation and synthesis that need to be solved [3]. The first challenge is to achieve uniform distribution of single atoms on support, preventing the aggregation of metal atoms. The second challenge is to precisely control the bonding and coordination environment of each metal atom. The existing preparation methods (Table 1) mainly include atomic layer deposition (ALD) [28], ball milling [29–31],

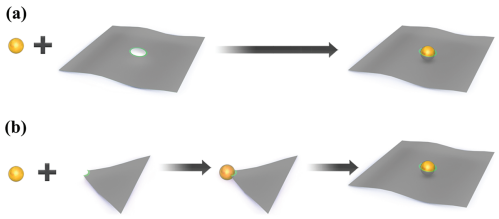

Fig. 2. Schematic diagram of (a) support anchoring strategy and (b) coordination design strategy.

incipient wetness impregnation [32–34], electrospinning [35,36], template-sacrificial approach [37–40], *etc.* According to the difference of interaction between single metal atoms and supports, synthesis strategies can be divided into two categories (Fig. 2). One is the support anchoring strategy (Fig. 2a), which mainly anchor single atoms onto existing supports through various methods; The other one is the coordination design strategy (Fig. 2b), which firstly design metal-organic precursors by coordinating N contained organic ligands with metal atoms, and then the N contained organic ligands can be polymerized to obtain stable support which is used to stabilize the metal atoms.

2.1. Support anchoring strategy

In this strategy, the supports such as N-doped graphene, carbon nitride, zeolitic imidazolate framework-8 (ZIF-8) are used to fix the single atoms by physical assistance methods and wet-chemistry methods. The physical assistance methods mainly include ALD [28,41], plasma sputtering method [42], microwave-assisted method [43,44], high temperature shockwave method [45], gas-migration method [46,47], photochemical reduction method [48,49], ball milling method [29,30,50], and electrochemical method [51,52]. The wet-chemistry methods mainly contain impregnation [32,33], deposition method [53–55], amine-induced-reduction method [56–58], surfactant-assisted method [59–62], cocoon silk chemistry method [63], and core-shell strategy [64].

2.1.1. Physical assistance methods

Atomic layer deposition: ALD method can be used to deposit single metal atoms on the surfaces of supports by alternately exposing the support materials to pulsed vapors of different precursors [41,65]. In this process, the distribution of single metal atoms on a supports can by precisely controlled with sequential or self-limiting surface reactions [41,66]. Sun *et al.* have synthesized the Pt/NGNs by the ALD process (Fig. 3a) [41]. They found that size and density of the Pt on the supports could be adjusted by changing the number of ALD cycles. Many single Pt atoms and small Pt clusters were uniformly dispersed on the surfaces of NGNs after 50 ALD cycles by using $MeCpPtMe_3$ as Pt precursor, and small Pt nanoparticles were also detected. After 100 ALD cycles, although many single Pt atoms and Pt clusters could still be observed, more Pt nanoparticles could be detected than 50 ALD cycles. The Pt loading rates for the Pt/NGNs after 50 and 100 ALD cycled were 2.1 and 7.6 wt%, respectively. Lu and co-workers also fabricated $Pd_1/g\text{-}C_3N_4$ and Pd_1/graphene SACs using the ALD method [28].

Gas-migration method: In recent years, preparation of SACs from bulk metal materials by gas-migration method has aroused the interest of many researchers due to its high stability and ease of mass production [46,47,67]. Li *et al.* synthesis the Cu-SAs/N-C with the gas-migration method by placing Cu foam and ZIF-8 in a porcelain boat [46]. Firstly, pyrolyzed ZIF-8 with defect sites and empty Zn nodes was prepared by pyrolyzing the ZIF-8 at high temperature (1173 K) in argon atmosphere. Then, NH_3 reacted with Cu foam to form volatile $Cu(NH_3)_x$ under NH_3 atmosphere. Finally,

Table 1
List of selected fabrication processes and characteristics method for M_1-N_x-C_y based SACs.

Strategies	Synthetic method	Catalyst	Metal loading [wt%]	Key characterization techniques	Ref.
Support trapping strategy	Atomic layer deposition	ALD100Pt/NGNs	7.6	ADF STEM, XANES, DFT	[41]
	Gas-migration method	Cd-NC-750 SACs	30.3	TEM, EXAFS, HAADF-STEM, XPS	[67]
	Plasma sputtering method	Pt/N-doped graphene	N.A.	HAADF-STEM	[42]
	Microwave-assisted method	Fe-N-C	0.93	TEM, SEM, Mössbauer spectrum	[69]
	High temperature shockwave method	Pt/C_3N_4	N.A.	HAADF, EXAFS, DFT	[45]
	Photochemical reduction method	Pt_1/NPC	3.8	STEM, DFT, XANES, EXAFS, XAS	[48]
	Ball milling method	Co-SNC	N.A.	EDX, HAADF-STEM, XANES	[71]
	Electrochemical method	PtSA-NT-NF	1.6	HAADF	[52]
	Impregnation method	1Ni/CN	1.0	HAADF-STEM, XPS, XANES	[75]
	Deposition method	Pt-SA/CTF-1	N.A.	HAADF-STEM, XANES, XPS	[76]
	Amine-induced-reduction method	Au_1N_x single-site/C_3N_4	0.7	HAADF-TEM	[57]
	Surfactant-assisted method	SA-Fe/NG	0.6	HAADF-STEM, EELS, XANES,	[59]
	Cocoon silk chemistry method	Co-ISA/CNS	9.2	HRTEM, HAADF-STEM, XAFS, EXAFS	[63]
	Core-shell method	SA-Fe/CN	0.9	HAADF-STEM, XRD, XANES, FT	[78]
Coordination design strategy	Electrospinning method	NiSA/PCFM	1.3	HRTEM, HAADF-STEM, XRD, EXAFS, FT	[35]
	Pyrolysis-free path	Fe-N-C	N.A.	HAADF-STEM, XAFS, XANES, DFT	[79]
	Cascade anchoring method	Fe-NC	8.9	HRTEM, HAADF–STEM, EELS, XAFS, XANES	[80]
	Template-sacrificial method	Co-N_x/C-800-AT	0.25	XRD, TEM	[39]
	Precursor-dilution method	Pt_1/N-C	0.43	STEM, HAADF-STE, XRD, EXAFS,	[81]
	MOF-derived method	Fe^{3+}-N-C	2.8	EXAFS, HAADF-STEM, XRD	[85]

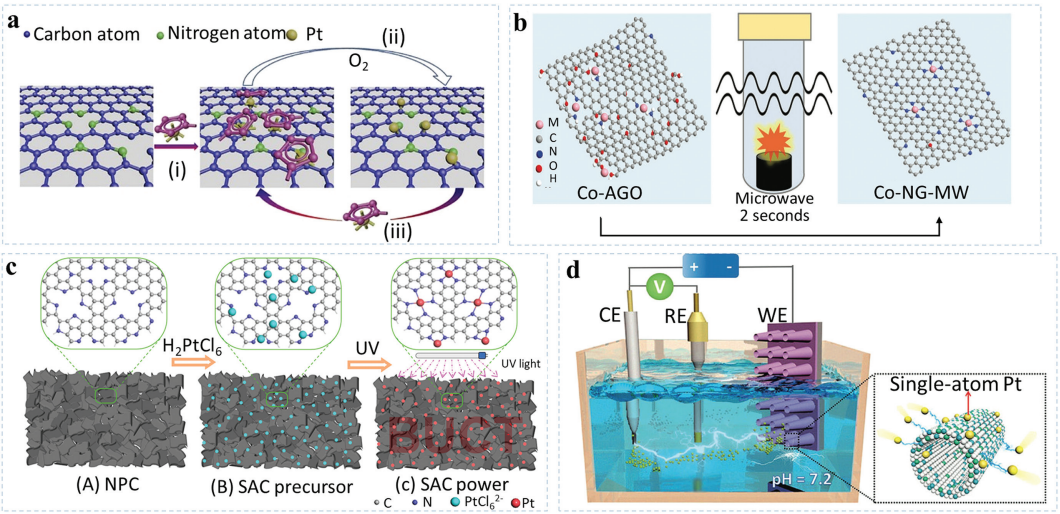

Fig. 3. Schematic illustration of preparation route to M_1-N_x-C_y based SACs by the physical assistance methods of support trapping strategy: (a) Preparation of Pt/NGNs using the ALD method. Reproduced with permission [41]. Copyright 2016, Springer Nature. (b) Preparation of Co-NG-MW by the microwave-assisted method. Reproduced with permission [44]. Copyright 2018, Wiley-VCH. (c) Preparation of Pt_1/NPC by the photochemical reduction method. Reproduced with permission [48]. Copyright 2018, American Chemical Society. (d) Preparation of PtSA-NT-NF by the potential-cycling method. Reproduced with permission [52]. Copyright 2017, Wiley-VCH.

the $Cu(NH_3)_x$ were captured by the defect sites of the pyrolyzed ZIF-8 to obtain the Cu-SAs/N-C catalysts. Wu and co-workers also prepared the M ISAS/NC (M = Cu, Mo, Sn) by the gas-migration method [47].

Plasma sputtering method: Plasma sputtering method is commonly used to prepare metal thin films or nanoparticles [42]. Yamazaki *et al.* used the plasma sputtering method to disperse single platinum atoms on the surfaces of graphene [42]. They found that pyridinic nitrogen was selectively doped in the graphene structure through the plasma sputtering in nitrogen gas atmosphere, and dense Pt single atoms (6.2×10^{13} cm^{-2}) were simultaneously formed on the N doped graphene.

Microwave-assisted method: The microwave-assisted method can not only reduce the reaction time, but also inhibit side reactions, so it is considered as an important approach for the synthesis of organic and inorganic nanomaterials [68,69]. Recently, many researchers have used this method to synthesize single atom catalysts [43,44]. Duan *et al.* synthesized a series of M (M = Co, Ni, Cu)-NG-MW by the microwave-assisted method (Fig. 3b) [44]. They firstly prepared the amine-functionalized GO (AGO) by mixing GO solution and aqueous ammonia, and then a certain amount of $CoCl_2$ was added to the AGO solution to obtain the M-containing AGO (M-AGO). Lastly, the solid M-AGO was microwave-irradiated in Ar atmosphere to obtain the Co-NG-MW with a Co loading rate of 1.10 wt%. Pérez-Ramírez *et al.* also used the microwave-irradiation-assisted deposition method to introduce palladium single atoms on the exfoliated graphitic carbon nitride (ECN) [43].

High temperature shockwave method: High temperature can promote the formation of stable bonds between metal atoms and substrates, but it usually causes atom agglomeration and is not suitable for temperature-sensitive substrates [45]. Hu *et al.* used controllable high-temperature (1500–2000 K) shockwaves to synthesize and stabilize Pt single atoms on CO_2-activated carbon nanofiber, reduced graphene oxide (rGO), nitrogen-doped carbon (C_3N_4) and TiO_2 substrates by a periodic on-off heating [45]. They found that the structural integrity of C_3N_4 can be maintained after the shockwave heating.

Photochemical reduction method: The photochemical reduction chemistry can effectively prevent nucleation and crystal growth in solution synthesis, and has been widely used in the synthesis of

nanomaterials and SACs [10,48,49,70]. Wu *et al.* reported a simple iced-photochemical reduction method that could reduce frozen chloroplatinic acid solution by using ultraviolet light to prevent atom aggregation and successfully obtained Pt atoms [70]. Then Pt atoms were deposited on graphene, mesoporous carbon, multi-walled carbon nanotubes, TiO_2 and ZnO nanowires. Wang *et al.* used ultraviolet radiation to directly reduce $PtCl_6^{2-}$ ions to Pt single atoms which were then deposited on the surface of NPC with a loading rate of 3.8 wt% (Fig. 3c) [48].

Ball milling method: Ball milling technology is an effective method to cut and reconstruct the chemical bonds of molecules or materials [30,71], and it has been wildly used in the preparation of SACs [29,30,50]. Bao *et al.* prepared graphene-embedded FeN_4 (FeN_4/GN) catalysts by confining the coordinatively unsaturated (CUS) single-iron sits in the graphene nanosheets (GNs) with the high-energy ball milling method [30]. Deng *et al.* also reported the preparation of MN_4/GN composites by ball milling of a MPc (M = Mn, Fe, Co, Ni, or Cu) and graphene [29].

Electrochemical method: The electrochemical method has been wildly used in preparation of nanomaterials and SACs due to the easy adjustment of metal particle size by changing the electrolytic concentration and the applied voltage [51,52,72]. Luo and co-authors used a potential-cycling method to synthesize PtSA-NT-NF [52]. As seen from Fig. 3d, a Pt foil, a Ni foam with CoP nanotube, and a saturated calomel electrode (SCE) were placed in phosphate buffer solution (PBS), and they were used as the counter electrode (CE), working electrode (WE), reference electrode (RE), respectively. The Pt weight percentage in the PtSA-NT-NF was 1.6%.

2.1.2. Wet-chemistry methods

Impregnation method: Impregnation is an effective method of anchoring individual atoms on the support surface [73–75]. The loading rate of a single metal atom mainly depends on the performance and density of the anchoring sites of the supports and the type of metal precursor. Wei and co-authors synthesized the Co_1/PCN by incipient wetness impregnation and pyrolysis processes [33]. The loading rate of Co in the Co_1/PCN was about 0.3 wt%. Yao *et al.* used the wetness impregnation method to prepare the Ru–N–C by impregnating Ru precursor ($RuCl_3$) into the phosphide carbon nitride, followed by a pyrolysis reaction in Ar atmosphere [32]. The loading rate of the Ru in the Ru-N-C was 1.0 wt%.

Deposition method: Deposition is a very effective method for preparing SACs [53–55,74,76]. Baek *et al.* reported a synthesis process of highly stable Cu–N–C with a very high Cu loading of 20.9 wt% [54]. Firstly, the $Cu(BTC)(H_2O)_3$ was used as precursor to synthesize the Cu doped nitrogenated carbon nanosheets, which were subsequently pyrolyzed at 800 °C in argon atmosphere and then treated by oxygen saturated acid to obtain the highly efficient and stable Cu–N–C catalyst. Li *et al.* also synthesized single Co sites on C_3N_4 by a deposition method [53].

Amine-induced-reduction method: Amine-induced-reduction method is a very interesting strategy because it can easily dope nitrogen atoms to the carbon support structure and firmly anchor the single metal atoms to the supports at the same time [22,56-58]. Hyeon and co-authors prepared the optimal Co-N_4 moiety incorporated in nitrogen-doped graphene (Co_1-NG(O)) by reducing the metal-adsorbed GO at 500 °C in NH_3 atmosphere [22]. Huang *et al.* synthesized a series of M-NHGFs (M = Fe, Co or Ni) by hydrothermally reducing metals adsorbed on 3D graphene hydrogel and incorporating the single metals into the graphene lattice under NH_3 atmosphere [56]. Liu *et al.* also reported an Au_1N_x single-site/C_3N_4 synthesized the amine-induced-reduction method [57].

Surfactant-assisted method: The surfactant can load metal atoms to form layered-like precursor, which can tightly anchor on the support surface and the metal atoms can be easily captured by the active sites of the support [59–62]. Pennycook *et al.* synthesized the NC-Cu SA by surfactant-assisted method, and the loading rate of Cu was 5.31 wt% [61]. They found that the NC-Cu SA exhibited very high catalytic performance of N_2 reduction with high Faradaic efficiency and NH_3 yield rate. Cao *et al.* firstly prepared the layered-like precursor by capturing Fe atoms with F127, and then the SA-Fe/NG was synthesized by pyrolyzing the precursor and g-C_3N_4 [59].

Cocoon silk chemistry method: Silk fibroin has a geometric sheet structure with many amino groups, which is beneficial for the construction of two-dimensional (2D) supports with rich N sites for anchoring single metal atoms [63,77]. Li *et al.* used *Bombyx mori* cocoons as raw materials to prepare M-ISA/CNS (M = Fe, Co, Ni) by cocoon silk chemistry method with four steps (Fig. 4a) [63]: (1) extraction of silk fibroin from *Bombyx mori* cocoons; (2) regeneration of the degummed silk fibroin in concentrated aqueous solution of metal salt; (3) salts-assisted pyrolysis at 900 °C to yield 2D porous nanosheets with isolated metal atoms; (4) removal soluble metal salts metal nanoparticles by acid etching. They found that the obtained Co-ISA/CNS have very large surface area of 2105 m^2/g and very high nitrogen content of 9.2 wt%.

Core-shell strategy: The core-shell strategy is an efficient route for preparing SACs [78]. Li and co-works synthesized SA-Fe/CN by this method with three steps (Fig. 4b) [64]: (1) preparation of α-FeOOH@PDA by coating α-FeOOH with carbonizing polydopamine; (2) carbonizing α-FeOOH@PDA at 700 °C under an inert atmosphere; (3) removing the unstable species by concentrated HCl. In the second step, CN shell was formed from the carbonizing polydopamine, and the α-FeOOH was reduced into Fe atoms, which were stably anchored on inner wall of the CN shell. The Fe content of the obtained SA-Fe/CN was about 0.9 wt%.

2.2. Coordination design strategy

2.2.1. Physical assistance methods

Electrospinning method: Electrospinning technology has the advantages of simple operation and process control, low cost, and a wide variety of spinnable materials to choose from. Therefore, it has become one of the most important methods for effectively preparing high-efficiency nanomaterials. He and co-workers used the electrospinning method to synthesize a Ni single-atom membrane catalyst (NiSA/PCFM) for CO_2 electroreduction (Fig. 5a) [35]. Firstly, precursor solution of ZIF-8, $Ni(NO_3)_2{\cdot}6H_2O$ and polyacrylonitrile were synthesized to primary fibers by electrospinning, and then the Ni atoms were anchored to the nitrogen-doped porous carbon in the calcine process. The Ni content in the NiSA/PCFM was 1.3 wt%. Wallace and co-workers also report a Sn single atoms nanofiber (Sn-CF) catalyst by electrospinning technique [36].

Pyrolysis-free path: At present, reported methods for preparing SACs generally include a high-temperature pyrolysis process, which often results in the aggregation of metal atoms and structure changes of support, thereby affecting the catalytic performance of SACs [79]. Peng *et al.* used the pyrolysis-free method to prepare Fe-N-C based SACs *pf*SAC-Fe-X (Fig. 5b) [79]. They firstly prepared the COF_{BTC} by assembling benzene-1,2,4,5-tetracarbonitrile with Fe centers, and then the *pf*SAC-Fe-X was obtained by assembling COF_{BTC} with graphene sheets. The *pf*SAC-Fe-X showed very excellent power density and cycling stability.

2.2.2. Wet-chemistry methods

Cascade anchoring method: The cascade anchoring strategy was used by Zhao *et al.* to prepare a series of M-NC SACs with a very high metal loading rate up to 12.1 wt% [80]. As seen from Fig. 5c, this strategy includes three steps: (1) chelation of metal ions

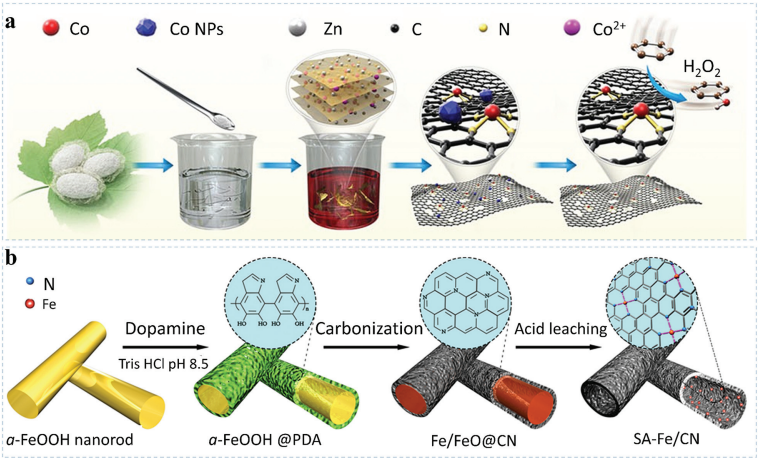

Fig. 4. Schematic illustration of the synthetic process for the M_1-N_x-C_y based SACs by the wet-chemistry methods of support trapping strategy: (a) Synthesis of Co-ISA/CNS by the cocoon silk chemistry method. Reproduced with permission [63]. Copyright 2018, Springer Nature. (b) Preparation of SA-Fe/CN using the core-shell strategy. Reproduced with permission [64]. Copyright 2017, American Chemical Society.

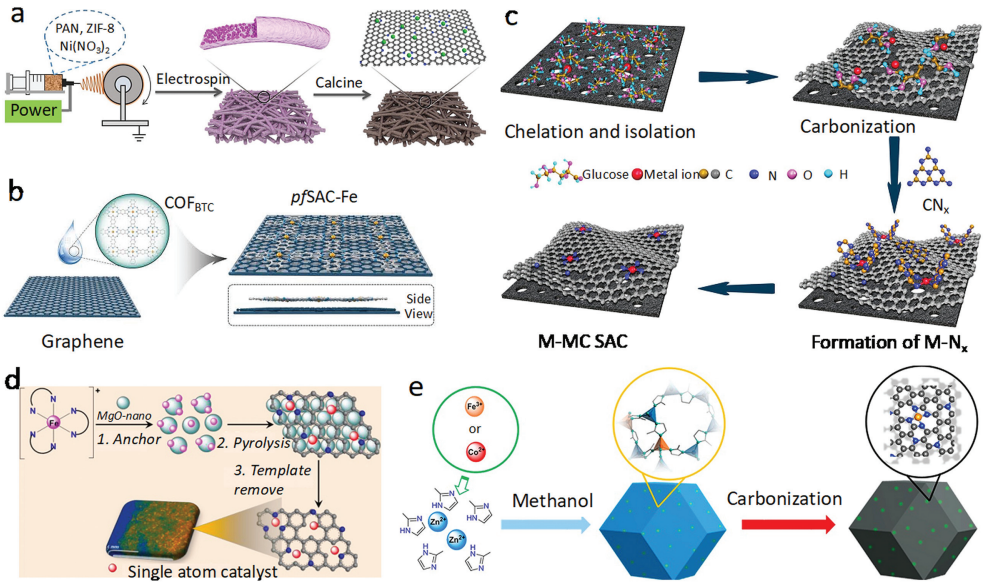

Fig. 5. Schematic illustration of the synthetic process for the M_1-N_x-C_y based SACs by the coordination design strategy: (a) Synthesis of NiSA/PCFM by the electrospinning method. Reproduced with permission [35]. Copyright 2020, Springer Nature. (b) Preparation of *pf*SAC-Fe catalyst by the pyrolysis-free path. Reproduced with permission [79]. Copyright 2019, American Association for the Advancement of Science (AAAS). (c) Synthesis of M–NC SACs by the cascade anchoring method. Reproduced with permission [80]. Copyright 2019, Springer Nature. (d) Preparation of Fe-N-C catalysts by the template-sacrificial approach. Reproduced with permission [37]. Copyright 2017, American Chemical Society. (e) Synthesis of Fe-N-C or Co-N-C by the MOF-derived method. Reproduced with permission [86]. Copyright 2018, American Chemical Society.

by chelating agent and isolation the chelates on the surface of O-rich porous carbon support; (2) carbonization of the chelated metal complexes at certain temperature to secure metal atoms; (3) formation of M-NC SACs at high temperature by integrating the M-N_x moieties into the pyrolyzed carbon layer. The Fe-NC and Ni-NC SACs showed very high electrocatalytic performance for O_2 and CO_2 reduction, respectively [80].

Template-sacrificial approach: The template sacrificial method is considered to be an effective strategy to avoid the aggregation of single metal atoms during the pyrolysis process in the preparation of SAC [37-39,51]. It generally involves three steps: (1) pre-impregnation of metal precursor on templates; (2) deposition of single metal atoms in the supports; (3) removal of the template by acid leaching. Zhang *et al.* prepared some Fe-N-C catalysts using the template-sacrificial approach at different temperature (Fig. 5d) [37]. The Fe loading rates of catalysts synthesized at 600 °C, 700 °C, and 800 °C were 1.8, 1.6, and 1.4 wt% respectively. Zhou *et al.* also used the template-sacrificial method to synthesize a robust Co–N_x/C-800-AT catalyst [39].

Precursor-dilution method: Precursor-dilution treatment can increase the distance between metal atoms dispersed on the polymer matrix, thereby preventing aggregation of single atoms in the pyrolysis process [81]. Ji and co-authors prepared 24 types of M_1/N-C using the precursor-dilution method [81]. They used the tetraphenylporphyrin (TPP) as the metal precursor, and the aggregation states of metal atoms (such as single atoms, nanoclusters, and nanoparticles) could be affected by the TTP concentration and pyrolysis temperature.

MOF-derived method: Metal-organic frameworks (MOFs) are very promising candidates to load single metal atoms due to their special structures. Recently, some MOF-derived SACs have been prepared with coordination design strategy [82–85]. Li and co-workers prepared Fe and Co-based M-N-C using chemically Fe- and Co-doped Zn-rich MOF (ZIF-8), respectively (Fig. 5e) [86]. The Fe

and Co ions were covalently bonded with 2-methylimidazole to form Fe- and Co-doped ZIF precursors, respectively. Then, the precursors were pyrolyzed to obtain the M-N-C catalysts, and the zinc atoms in the ZIF acted as spacers to avoid the aggregation of Fe and Co atoms. Chen and co-workers prepared a Ir-SAC using the ZIF-8 as active site host and the Ir acetylacetonate as guest, respectively [82]. The Ir-SAC has exceptionally high oxygen reduction reaction activity.

3. Identification of single metal atoms in the M_1-N_x-C_y based SACs

Confirming the existence and spatial distribution of isolated metal atoms is critical to analyzing the relationship between structure and performance of the SACs [73]. Through advanced characterization technology, the active site of the SACs can be identified, which is very important to the development of highly active SACs. Scanning transmission electron microscopy (STEM) and scanning tunneling microscopy (STM) are the general characterization techniques for analyzing surface morphology of SACs. Spectroscopy data obtained by spectroscopic techniques such as X-ray absorption spectroscopy (XAS), X-ray photoelectron spectroscopy (XPS), infrared spectroscopy (IR) can provide more valuable information about the active sites of SACs [87]. Because the M_1-N_x-C_y based SACs have an ideal model structure, theoretical calculation models such as density functional theory (DFT) can be used to effectively analyze the structure-performance relationship and catalytic mechanism [87].

3.1. Microscopic techniques

3.1.1. Scanning transmission electron microscopy

STEM is a convincing and intuitive characterization technique with atomic resolution to image isolated single atoms of the SACs, which can directly confirm the existence and spatial distribution of isolated metal atoms on the supports [87–89]. Annular dark field (ADF) and high-angle annular dark field (HAADF) are the two common imaging modes of STEM [90]. Huang *et al.* prepared a series of M-NHGFs, which were imaged by the ADF-STEM. The isolated Ni, Fe, and Co ions (bright dots) embedded in the graphene sheets were clearly observed, and they coordinated with N atoms to form MN_4C_4 structures [56]. Bao *et al.* used the High-angle annular dark field scanning transmission electron microscopy (HAADF-STEM)to characterize the FeN_4/GN catalysts (Figs. 6a and b), which shows the atomic size and well distribution of the isolated Fe atoms (bright dots) on the graphene sheets [30].

3.1.2. Scanning tunneling microscopy

STM is an atomic-level surface imaging technology. According to the change of tunnel current, we can get the information of the small fluctuation of the sample surface. If we scan the x-y direction at the same time, we can directly get the three-dimensional surface morphology of the sample with the lateral resolution of 0.1 nm and the depth resolution of 0.01 nm [89]. STM allows scientists to observe and locate individual atoms on the supports, and it is an effective tool for investigating SACs. Bao *et al.* used the LT-STM (low-temperature scanning tunneling microscopy) to characterize FeN_4/GN (Fig. 6c), and obtained valuable information about the atomic and electronic structure of Fe center (FeN_4) in the graphene support [30]. The Fe atoms were displayed as bright spots, which exhibited a higher apparent light than other C atoms. The STM simulation (Fig. 6d) is consistent with the STM image, implying that the density of states of neighboring atoms can be largely affected by the Fe atoms. Bao and co-works also used the STM to analyze the Cu-N sites in the graphene supports, and get many information of the Cu-N center [91].

3.2. Spectroscopic techniques

3.2.1. X-ray absorption spectroscopy

XAS is a powerful method to evaluate the interaction information between the single metal atoms and their neighboring atoms, and to obtain the information about electronic state and structure of the material [92–94]. XAS generally includes X-ray absorption near-edge spectroscopy (XANES) and Extended X-ray absorption fine structure (EXAFS) [6]. According to the characteristics of peaks and shoulders near or on the edges of the XAS, information about the chemical state and geometric structure of single atoms can be obtained by the XANES [87]. While EXAFS can supply valuable information on the coordination number and distance of the absorbed atoms and the nearby backscatter [89,92]. Usually, standard samples are required for comparison. Zhao and co-workers used the XAS to characterize the Fe-NC SAC (Figs. 6e-h) [80]. They found that the XANES and the first derivative XANES spectra of the Fe-NC SAC were distinct from those of the Fe foil (Fig. 6e), while similar to those of the FePc, indicating that the Fe-NC SAC has ideal coordinated sites (Fe-N_4). From the FT-EXAFS spectra (Fig. 6f), Fe-NC SAC showed a very strong peak at about 1.50 Å for Fe-N coordination, while no apparent peaks for Fe-Fe coordination could be observed. From the WT (wavelet transform) of the k_3-weighted EXAFS data (Fig. 6g), the WT maximum at about 4.5 $Å^{-1}$ for the Fe-NC SAC was similar to that of the FeP, but was distinct from the Fe foil, which also proved the existence of Fe–N bonding without Fe–Fe bonding in the catalysts. From the results of FT EXAFS fittings in *R*, *q*, and *k* spaces, the average coordination number for Fe-N was 4.3 and the average bond length for Fe–N was 1.99 Å. The N K-edge NEXAFS spectrum showed three peaks at 398.8, 399.8, and 401.8 eV (Fig. 6h), which could be assigned to pyridinic state, Fe–N bonding, pyrrolic, respectively.

3.2.2. X-ray photoelectron spectroscopy

XPS is a very common technique to obtain the information of elemental composition and content, chemical state, molecular structure, and chemical bonds of various materials. This technique can be used to analyze the electronic environment and coordinating information the isolated atoms in SACs. Zhao *et al.* used the XPS technique to characterize the Fe-NC SAC (Fig. 6i) [80]. The N 1s signals at 398.3, 399.5, 400.4, 400.9, and 401.7 eV for the Fe-NC SAC could be assigned to pyridinic-N, Fe-N_x, pyrrolic-N, graphitic-N, and oxidized-N, respectively. The reference iron phthalocyanine (FePc) also had a peak at about 399.5 eV, which indicated the existence of N in the chemical state similar to Fe-N_x in the FePc.

3.2.3. Infrared spectroscopy

IR spectroscopy has played a key role in the characterization of SACs because it can directly monitor the chemical interaction between adsorbent molecules and the solid surface [92]. By detecting changes in the frequency and intensity of chemical bonding vibrations, the physical and chemical properties of the catalytically active center can be deduced, and qualitative and quantitative information on isolated atoms of SACs can also be obtained [95]. Wei *et al.* used the IR spectra to characterize the Co_1/PCN and reference PCN catalyst under the open-circuit condition, and they found that the O–H stretching peak became much stronger for Co_1/PCN, indicating considerable adsorption of hydroxyl species on the isolated Co site [33]. Hyeon *et al.* also applied the IR spectroscopy to analyze the Co_1-NG(O) and Co_1-NG(R) [22].

3.3. DFT calculations

DFT has been wide used to study the properties of molecules and condensed matte because it is a very useful quantum mechanical method for studying the electronic structure of multi-electron

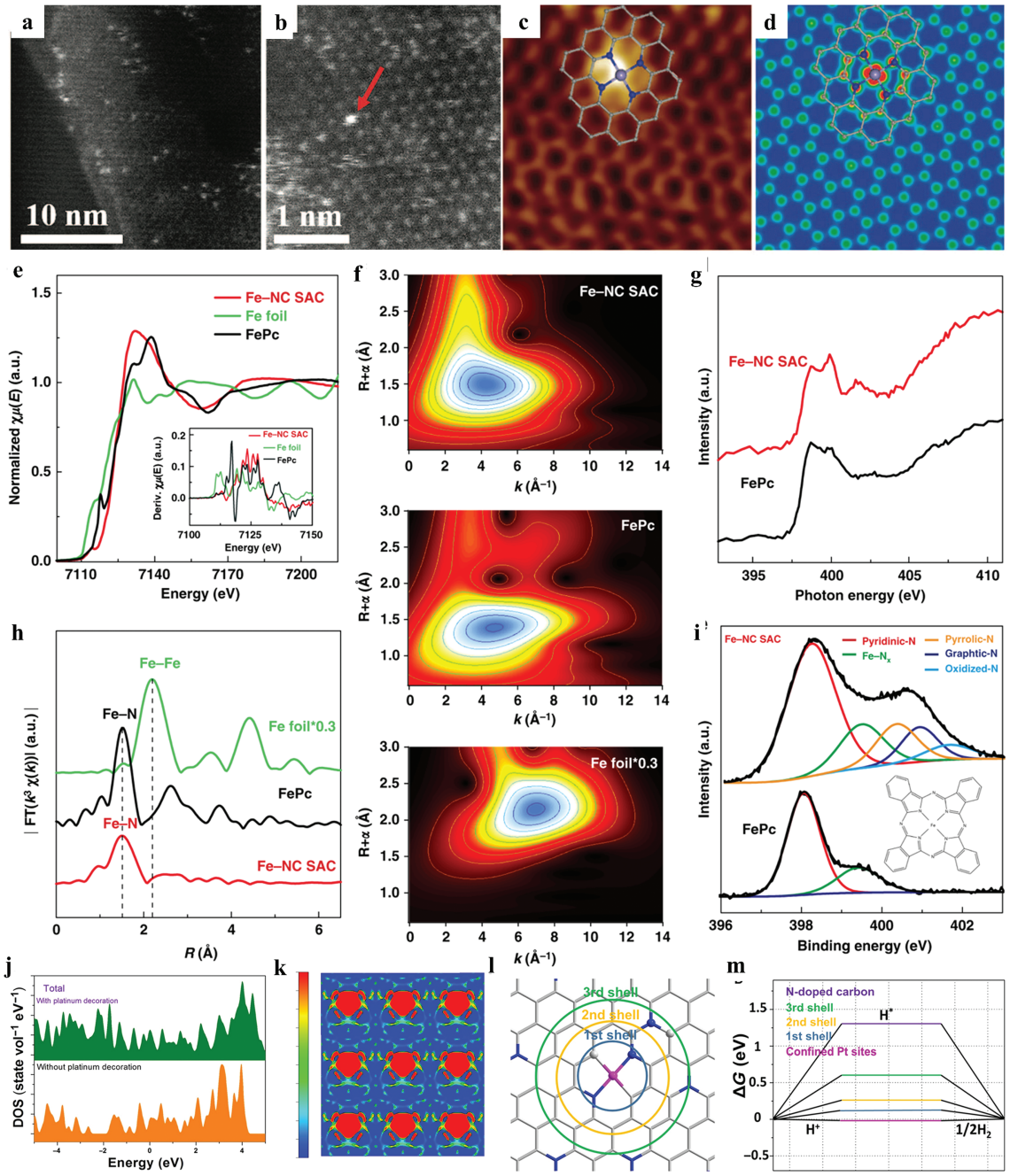

Fig. 6. Atomic structure characterizations of M_1-N_x-C_y based SACs: (a, b) HAADF-STEM and (c) LS-STM images of FeN_4/GN-2.7. (d) Simulated STM image for (c). (a-d) Reproduced with permission [30]. Copyright 2015, American Association for the Advancement of Science (AAAS). (e) Fe *K*-edge XANES spectra, (f) FT-EXAFS spectra, (g) WT of the k_3-weighted EXAFS data, (h) N K-edge NEXAFS spectra, and (i) deconvoluted N 1s XPS spectra of Fe-NC SAC and reference samples. (e-i) Reproduced with permission [80]. Copyright 2019, Springer Nature. DFT calculation results: (j) DOS, (k) calculated distribution of charge density, (l) schematic description of coordination shells for the isolated Pt on graphene, (m) ΔG_{H^*} on pure and Pt-decorated graphene. (g-m) Reproduced with permission [104]. Copyright 2018, American Association for the Advancement of Science (AAAS).

systems [22,96]. In recent years, with the development of SACs, DFT is an important tool for studying SACs [97–99]. It is mainly used to design the optimal catalyst, calculate the catalytic activity, and simulate the catalytic mechanism [88,100,101].

3.3.1. Optimal catalyst design

The DFT calculation can predict the most stable configuration of single atoms on the supports, and can provide some valuable information about inherent structure and characteristics of the SACs [95]. First, the quantitative relationship between the adsorption energy and the physical and chemical properties of the catalyst can be established by DFT, and then the preparation method can be optimized to prepare the catalysts with the best catalytic performance [88]. Wang *et al.* evaluated the relative stabilities of the Mn-N_x doped graphene catalysts by DFT calculation, and found that the Mn-N_3/M, Mn-N_4/D, and (Cyan or Pyri) Mn-N_4/D were the most stable structures in the SACs [102]. Esrafili and Nejadebrahimi used the DFT to analyze the geometry, electronic structure, and stability of single Co atom incorporated N-graphene. They found that both of CoN_3-Gr and CoN_4-Gr were energetically stable substrates and CoN_3-Gr had a higher reactivity than CoN_4-Gr [103].

3.3.2. Catalytic activity calculation

To identify the catalytically active sites, the interaction between single atoms and supports can be described by density of states (DOS), charge density map, and Bader charge analysis [88]. Lou and co-workers used the DFT calculations to analyze the catalytic activity of Pt-decorated graphene [104]. From the results of DOS (Fig. 6j), some hybridized electronic states in Pt@PCM could be observed, which mainly due to the hybridization between Pt and the neighboring nonmetal atoms. From Fig. 6k, the charge density around Pt atoms is large, which indicates that the single atom Pt in the catalyst is beneficial to the charge density distribution, thereby enhancing the catalytic activity. What is more, from Figs. 6l and m, we can find that the Pt and neighboring C and N atoms might be the active sites for HER.

3.3.3. Catalytic mechanism simulation

We can use the DFT calculation to explore the possible mechanism of catalytic reaction by estimating the electron transfer reaction through valence electron structure [10,95]. Shang introduced the DFT calculation used in Carbon-based single atom catalyst [105]. Liu and co-authors explored the photocatalytic mechanism of water splitting on *x*Pd/C_3N_4 by DFT calculations [55]. They found that when C_3N_4 is loaded with Pd_1, the highest occupied molecular orbital (HOMO)of Pd_1/C_3N_4 consisted of charge densities from single Pd atoms and the lowest unoccupied molecular orbital (LUMO) of Pd_1/C_3N_4 consisted of charge densities from C and N atoms of C_3N_4 support, indicating a very strong spatial separation of e^- and h^+. They also found that the e^- mainly accumulated in the C_3N_4 support and h^+ mainly accumulated in Pd atoms. The routes on single atoms for H_2 evolution are as follows: the electrons firstly transfer from C_3N_4 support to single Pd atoms and then reduce H^+ to H_2.

3.4. Other techniques

In addition to the above characterization techniques, X-ray diffraction (XRD), Mössbauer spectroscopy, and Raman spectroscopy were also usually used to analyze the SACs. Hu *et al.* used the XRD to characterize the Fe^{3+}-N-C, and no peaks of any Fe and Zn crystalline species were observed, indicating the isolated Fe sites [85]. Zhang and co-workers studied three Fe-N-C samples by Mössbauer spectroscopy [37]. They found that aggregates of Fe^0 particles were observed in Fe-N-C-800, and only single Fe atoms were detected in Fe-N-C-600 and Fe-N-C-700. Raman spectroscopy is also a powerful technique that can analyze the electronic structure of single metal atoms supported on two-dimensional materials [95]. Moreover, characterization techniques such as energy dispersive spectrometer (EDS), scanning electron microscope (SEM), and N_2 absorption can also provide the fundamental physical and chemical properties of SACs [89]

4. Environmental applications

The developments in industrialization, rapid growth of population, and accelerated urbanization have significantly contributed to severe environmental pollutions [1], such as air pollution, water pollution, and soil pollution, which have seriously threatened organisms and humans health [106]. Catalytic technology is one of the most powerful ways for the remediation of environmental pollutions because it can thoroughly convert toxic pollutants into low-hazard or environmentally friendly substances [1,107,108]. SACs have high catalytic activity and have some applications in harmful gas treatment [11,109], water purification [110–112], sensors [113], disinfection [114]. However, the M_1-N_x-C_y based SACs have only been used in harmful gas treatment [115–119]. and water purification [120–125].

4.1. Management of harmful gases

There are many types of harmful gases emitted from industrial production processes, such as CO_x, NO_x, H_2S, halides, and hydrocarbons. Industrial waste gas and flue gas are mostly gas mixtures. Purification methods of gas mixtures can generally be divided into three categories according to different principle of action: absorption, adsorption and catalytic conversion. Among them, the catalytic conversion method uses catalysts to convert pollutants into harmless substances, or even useful by-products, or into substances that are easier to separate and remove from the gas stream. And in a recent article, Lei and co-workers introduced SACs used in gas sensors [126]. Benefiting to the superior electronic properties of single atoms, the SAC-based sensors show excellent gas sensing capabilities long-term stability to harmful gas such as H_2S, HCHO, NO_2. Cui's article [127] sketched out the recent progress for catalysis of acetylene hydrochlorination reaction without mercury to address the environmental-benign synthesis. The M_1-N_x-C_y based SACs were studied for conversion of CO [115,116,128], NO [117,119,129,130], and H_2S [118,131].

4.1.1. Conversion of CO

Catalytic oxidation of CO to CO_2 is an important method to solve the environmental pollution problems caused by automobile exhaust and industrial processes [115,132]. To date, various SACs with high reactive activity, selectivity and durability have been successfully prepared for conversion of CO [133]. M_1-N_x-C_y based SACs were proven to have good stability and catalytic activity for CO conversion using the first-principle calculations [115,116,128]. Dai and co-authors used the first-principles method to study the structural, electronic and catalytic properties of the Si-GN_4[115], and found more stable O_2 adsorption than CO on the surface. The pre-adsorbed O_2 could firstly react with CO to form OOCO with a small energy barrier of 0.57 eV, and then the atomic O_{ads} could react with the physisorbed CO to form CO_2 with an energy barrier of 0.72 eV. Wang and co-authors studied the potential usage of Co/g-C_3N_4 for CO oxidation [116]. They found that the kinetic energy barriers for all possible CO oxidation pathways were in the range from 0.21 eV to 0.59 eV, indicating the superior catalytic activity of the Co/g-C_3N_4. Dai and co-workers found that the coadsorption of two gas molecules (NO/O_2, CO/O_2, 2NO and 2CO) on N_3-graphene-Pd were more stable than the single gas molecule [128]. The different rate-limiting steps for termolecular Eley-Rideal and Langmuir-Hinshelwood mechanisms have relatively small energy barriers ($<$ 0.7 eV), indicating that the N_3-graphene-Pd could be used as an efficient catalyst for toxic gases removal.

4.1.2. Conversion of NO

Nitric oxide (NO) is a toxic gas that is colorless, odorless and hardly soluble in water. Some researchers have confirmed that the M_1-N_x-C_y based SACs could effectively catalyze the conversion of NO into non-toxic or low-toxic substances [117,119,128-130]. Ding and co-authors conducted a theoretical study on catalytic oxidation of NO and Hg^0 by Pd_{sac}/g-C_3N_4, and the oxidation products, NO_2 and Hg^{2+}, could be easily removed by the WFGD [129]. Almost all equilibrium constants for NO oxidation were more than 10^5, implying the NO oxidation reactions are irreversible. The lowest activation energies of NO and Hg^0 were 0.46 eV and 1.81 eV, respectively. Chen *et al.* studied the potential of utilizing Co-N_4/graphene for electrochemical conversion of NO by the DFT computations [117]. The NO molecules could be firstly activated on the Co-N_4 sites, and then they could be converted into NH_3 at low coverages or N_2O at higher coverages. Besides, the onset potential was about −0.12 V, which was comparable to those on well-established Pt-based catalysts. The results indicated that the Co-N_4/graphene showed a high efficiency for NO removal. In another interesting

article, authors studied the relationship between single atom elements and the adsorption efficiency to NO and NO_2 in gas sensor [134]. They found that different metal single atom (Mn, Fe, Co and Ni) would affect the toxic-gas reduction reactions which associated change in the magnetic state of elements.

4.1.3. Conversion of H_2S

H_2S is one of the most toxic and foul-smelling gases [135]. Low concentrations of H_2S have effects on the eyes, respiratory system and central nervous system [136]. With the continuous improvement of environmental standards, it is very important to develop green technologies to transform H_2S into useful products. Direct catalytic oxidation of H_2S to S is the most promising method because it can achieve complete H_2S removal at a relatively low cost, and the useful elemental sulfur can be obtained [118]. Jiang *et al.* synthesized the Fe-CN-NHχ by embedding isolated Fe-Nχ sites in g-C_3N_4 [118]. The Fe-CN-NH_5 showed the highest H_2S conversion of about 100% at 210 °C, which was far better than that of bulk g-C_3N_4. The sulfur selectivity was close to 100% at temperature below 180 °C, and it could maintain *ca.* 98.2% at 240 °C. No obvious decrease of catalytic activity for Fe-CN-NH was observed after 180 h of reaction. These results indicated that the Fe-CN-NH_5 is a suitable candidate for efficient removal of H_2S.

4.2. Water purification

SACs are very suitable for the removal of pollutants in water because of their unique chemical and structural properties. The M_1-N_x-C_y based SACs have quickly become a novel material under spotlight in technologies of Fenton-like catalysis [12,121,137-139], photocatalytic degradation [120,122,123,125,140-143], and electrochemical filtration [124].

4.2.1. Fenton-like catalysis

Traditional homogeneous Fenton catalysis process can degrade most organic pollutants [144]. However, the drawbacks of narrow work pH range, accumulation of ferric oxide sludge, and low H_2O_2 utilization rate significantly limit its wide-spread application [145]. In recent years, the heterogeneous Fenton-like catalysis-based SACs with high catalytic activities and a wide work pH range has been developed [12,110,121,137-139,146,147]. Zhou and co-authors prepared the Fe_{SA}-N-C for efficient catalytic oxidation of bisphenol A (BPA) *via* peroxymonosulfate (PMS) activation [137]. 100% removal of BPA (20 mg/L) could be observed in 30 min for Fe_{SA}-N-C/PMS (0.15 g/L Fe_{SA}-N-C and 0.4 g/L PMS), which was higher than that of Fe_{NP}-N-C/PMS, indicating the unique catalytic activity of the single Fe sites. The Fe content in the Fe_{SA}-N-C could affect the catalytic activity for BPA degradation, and the Fe_{SA}-N-C-20 (20 mg Fe $(NO_3)_3{\cdot}9H_2O$) showed remarkable performance for PMS activation because it has a large number of Fe-N_x active sites. Zhang *et al.* synthesized the FeCo-NC at different calcination temperatures, and found that the FeCo-NC-2 (calcined at 650 °C) showed the highest performance for PMS activation [12]. For FeCo-NC-2, the 100% removal of BPA (20 mg/L) could be observed in 4 min (0.1 g/L FeCo-NC-2 and 0.2 g/L PMS). Zhu *et al.* synthesized a Co-N-C catalyst for activating PMS [121]. They found that the Co-N-C calcined at 900°C could completely remove BPA (80 mg/L) in 3 min (0.5 g/L Co-N-C-900 and 0.3 g/L PMS). Chen *et al.* prepared the SA-Cu/rGO for the degradation of SMX (sulfamethoxazole) by activating PMS [138]. The degradation kinetic of the SA-Cu/rGO/PMS was about 3.9 times faster than that of the rGO/PMS. The SA-Cu/rGO/PMS system showed very high mineralization ability because over 99% of the TOC was eliminated within 120 min. Apart from this, a dual reaction sites SAC was prepared for PDS activation and organics decomposition in Shang's article [148]. SMX would be well adsorbed *via* benzene ring binding for the abundant conjugated π-π sp^2 structured carbon and the Fe-N_4 sites also has strong binding adsorption to PDS. The adsorption of SMX is beneficent to minimize the migration distance of the ROS. Meanwhile, PDS activation is accelerated due to the combined between Fe-N_4 sites and PDS molecular. Because of this, the organics decomposition process of the reconstructed Fe-SAC is significantly higher (~6 times) than the conventional Fe-SAC (Fig. 7a). In another research, a SAC-based PMS system was used to the degradation of bisphenol A (BPA) and metronidazole (MNZ) [149]. Radical oxidation ($SO_4^{\bullet-}$ and $HO^{\bullet}$) and nonradical electron transfer pathway (ETP) all co-existed in the Co−N_4−C/PMS system according to the quenching experiments. From density functional theory calculations, the Co-N_4 active sites increased the adsorption and activation of PMS which improve the charge transfer to PMS to evolve radicals. A Fe-SAC located on carbon nitride used in flow-through filter was reported by Professor Zhang [150]. With the $FeCN_5$ activate sites and ultrafast H_2O_2 activation, methylene blue oxidation rate can reach to 59.43 mg L^{-1} min^{-1} *via* direct and nearly 100% pollutant degradation and stability over 320 h in actual wastewater solution (Fig. 7b). For comparison, Xiong and co-workers found that the removal rate constant of *p*-nitrophenol (PNP) by micro zero-valent was 0.1779 min^{-1} [151]. Liang [152] and team-workers investigated catalytic activity of Co-SACs from the coordination number. They found that the coordination N with metal single atom could modulate electron distribution and the decrease of nitrogen coordination number will lead to higher specific activity of Co-N_x.

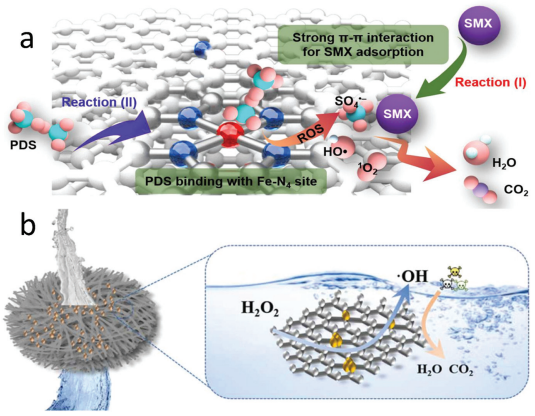

Fig. 7. (a) Proposed mechanism of DFeNC catalyzing PDS for SMX degradation. Reproduced with permission [148]. Copyright 2020, Elsevier B.V. (b) Proposed mechanisms of the $FeCN_5$-H_2O_2 catalytic system for ·OH generation. Reproduced with permission [150]. Copyright 2020, Elsevier B.V.

4.2.2. Photocatalytic degradation

The photocatalysis technique is an effective method for the removal of pollutants because of its easy operation and low cost without secondary pollution [141,153]. Many semiconductor materials, such as TiO_2 [153,154], $BiFeO_3$ [155], $BiVO_4$ [156], and g-C_3N_4, were used as photocatalysts to degrade pollutants in water [157]. However, the catalytic efficiencies of these materials Pt_1@MIL are usually not high due to their slow charge mobility and fast recombination of electron-hole pairs [107,123]. Anchoring single metal atoms to the photocatalysts is an effective method to modulate their optical, conductive, and magnetic properties, thereby improving their catalytic efficiencies [120,122,123,125,140-143]. Zhao *et al.* prepared the Ag/mpg-C_3N_4 for degradation of BPA with presence of PMS under visible light [123]. For Ag/mpg-C_3N_4, the100% removal of BPA (20 mg/L) and 80% removal of TOC could be observed within 60 min under visible light ($\lambda > 400$ nm, 0.1 g/L Ag/mpg-C_3N_4 and 1 mmol/L PMS). Wang and co-authors found that the MoS_2/Ag/g-C_3N_4 showed excellent and rapid degradation

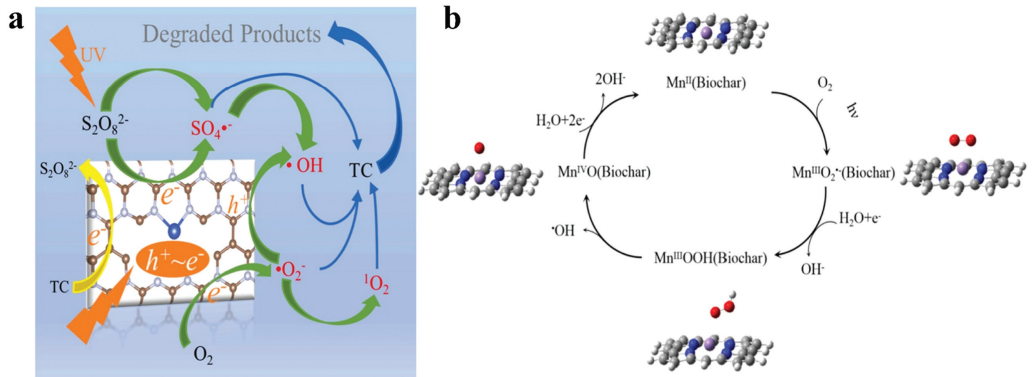

Fig. 8. (a) Degradation mechanism of TC by SAS-Cu/PS/Light system. Reproduced with permission [158]. Copyright 2022, Elsevier B.V. (b) The reaction path of Mn-SACs. Reproduced with permission [159]. Copyright 2022, American Chemical Society.

of tetracycline with presence of PMS [141]. About 98.9% of tetracycline (20 mg/L) was removed in 50 min under visible light irradiation (0.2 g/L MoS_2/Ag/g-C_3N_4 and 0.1 mmol/L PMS). Guo *et al.* reported that the FeN_x/g-C_3N_4 showed improved activity and stability in degrading MB, MO, RhB, and phenol under visible light [120]. Liu *et al.* synthesized the SDAg-CQDs/UCN which showed a highly enhanced photocatalytic activity for naproxen under UV, vis, and NIR irradiation [140]. The degradation rate of the SDAg-CQDs/UCN was about 10 times higher than that of the UCN. Carbon nitride (CN) material loaded single-atomic-site Cu catalyst (SAS-Cu) was synthesized which improved the charge transfer and separation efficiency in Liu's paper [158]. The SAS-Cu catalyst greatly improved the utilization of oxidant that the reaction rate constant of SAS-Cu is much faster than that of CN (4.5 times) and the remove efficiency of tetracycline (TC) could reach 82.5% in 30 min with LED illumination. The main degradation mechanism of TC by SAS-Cu/PS/Light system has been shown in Fig. 8a. In another article, Cui and co-workers dispersed Mn atoms in the carbon matrix formed a $Mn-N_4$ structure [159]. The $Mn-N_4$ site exhibited a high photooxidation efficiency for degradation of organic pollutants with photoelectrons transformation between adsorbed O_2 and Mn active center to generate reactive oxygen species (Fig. 8b).

4.2.3. Electrochemical filtration

Electrochemical filtration combines the advantages of electrochemical technology and membrane filtration technology, and it has great application prospects in the water treatment process [154]. The removal or degradation of pollutants in the systems can be controlled by using different potentials onto the conductive membrane [124]. The performance of the electrochemical filtration can be affected by the activity of electrocatalysts on the conductive membranes [124]. For comparison, a highly efficient electrolysis-ozone process for *N-N* dimethylacetamide degradation was introduced by Xiong *et al.* [160]. Chew *et al.* have demonstrated that the SACs (NG-Co) can be used as highly active conductive membrane for improving the practicality of electrochemical filtration [124]. The NG-Co showed 99.5% rejection of methyl blue at 2.5 V, and retained > 90% of activity after 5 cycles. The TOFs of the NG-Co for methyl blue and Rhodamine B were 13.5 and 16.6 times higher than that of Co oxides nano-catalyst.

5. Outlook

From the above discussions, it is obvious that SCAs inherit the merits of homogeneous and heterogeneous catalysts, thereby building a bridge between them. The M_1-N_x-C_y based SACs show some excellent new features for enhancing their performance in various applications because of its unique electronic and structural properties. Although great attention has been paid on the M_1-N_x-C_y based SACs, this field is in its infancy and there are still several challenges existed. Therefore, it is necessary to develop novel preparation strategies, study the fundamental mechanisms, and therefore expand their practical applications.

5.1. Preparation strategy exploration

The electronic properties and catalytic performance of SACs are significantly affected by the structure and composition of the support [6,17,18]. For the M_1-N_x-C_y based SACs, the first challenge is how to accurately control the coordination structure of the single atoms through innovative preparation methods to achieve the purpose of improving its catalytic activity and selectivity. It is a great challenge because the catalytic activity of the single atoms is controlled by adjusting the number and coordination method of the nitrogen and carbon atoms. In addition, the coordination environment of the single atoms can change the interaction of the SACs with different reaction substrates, thereby improving the selectivity of the SACs. However, for some existing preparation methods, the pyrolysis process usually causes various vacancies and surface reconstructions of N-doped carbonaceous materials, making it very difficult to obtain the exact coordination structure of the single metal atoms. Therefore, there is an urgent need to develop some non-pyrolysis and simple methods for obtaining M_1-N_x-C_y based SACs with precise coordination environment. The second challenge is how to prevent the aggregation and oxidation of metal atoms during the preparation process. The aggregation and oxidation of metal atoms are crucial factors for the catalytic performance of SACs. However, some existing preparation methods usually include a pyrolysis step, which easily leads to the aggregation and oxidation of metal atoms. Therefore, advanced preparation methods are needed to improve the dispersion of metal atoms and prevent them from being oxidized. The third challenge is how to obtain an ideal loading rate of single metal atoms. In theory, increasing the loading rate of single metal atoms can enhance the catalytic efficiency of the M_1-N_x-C_y based SACs. However, increasing the loading rate may also cause the metal atoms to aggregate more easily. Therefore, it is necessary to further optimize the preparation method to effectively increase its loading capacity while inhibiting the aggregation of metal atoms. Additionally, for some catalytic reactions (*e.g.*, metal-air batteries, water splitting), the development of dual- or multi-functional catalysts is particularly meaningful. The biggest challenge in preparing this new type of catalyst is how to stably fix two or more types of metal atoms on a suitable support. What is more, exploring simple and convenient methods to synthesize SACs on a large scale is also crucial to its practical application in industry.

5.2. Mechanism study

Although many scholars have studied the synthesis and application of M_1-N_x-C_y based SACs, the basic mechanism of the coordination process of single atoms, the synergistic effect of single metal atoms and supports, and the interactions between SACs and substrates during the catalysis process remain unclear. At present, the mechanism analysis on how to effectively improve the coordination environment of a single metal atom by controlling the reaction conditions is not thorough enough. Besides, the process and mechanism of the synergy between single atoms and supports is more through speculation. In addition, the thermodynamic equilibrium of the interaction between M_1-N_x-C_y based SACs and the substrate remains to be further explained. The DFT calculations have been applied to design the optimal catalyst, calculate the catalytic activity, and simulate the catalytic mechanism [88,97,98,100]. However, future work needs to combine the results of these theoretical calculations to prepare a catalyst with excellent performance by optimizing the preparation conditions, and to analyze the conversion pathway and mechanism of the substrate on the M_1-N_x-C_y based SACs.

Another effective strategy to accelerate the progress of mechanism research is to use advanced characterization methods. Some characterization techniques such as STEM and EXAFS can analyze the morphology, spatial distribution of single atoms on the support, and information about their coordination structure, which can help us to fully understand the M_1-N_x-C_y based SACs. However, most of the current attention has been paid to characterization before the catalytic reaction. In-depth understanding of the geometry and structural transformation of active sites in the catalytic process is essential for optimizing the design of the catalyst and elucidating its reaction mechanism. Therefore, it is necessary to use more advanced technology, powerful kinetics research, and theoretical calculations to analyze the M_1-N_x-C_y based SACs in the catalytic process and after the catalytic reaction. Based on that, the structure-activity relationship of the SACs will be obtained, which is very important for feedback preparation of high-performance M_1-N_x-C_y based SACs.

5.3. Application expansion

As mentioned above, M_1-N_x-C_y based SACs are highly desirable for the use of catalytic technology in various applications. To date, the environmental applications for the M_1-N_x-C_y based SACs is relatively small, and they mainly focus on the removal of organic pollutants from gases and water. Thus, their potential applications in the field of environment urgently need to be expanded, such as antimicrobial, removal of inorganic pollutants, and chemical sensors.

Although some existing M_1-N_x-C_y based SACs have excellent catalytic activity and selectivity, they only meet the basic requirements of being good industrial catalysts. The current main challenge is the stability of the M_1-N_x-C_y based SACs, because industrial applications require the catalyst to remain stable for months or years. Therefore, the application stability of the M_1-N_x-C_y based SACs in actual industry needs to be further demonstrated. In addition, the balance between the cost and performance of the SACs is also an issue that needs to be considered in the application process.

6. Conclusions

In summary, this critical review highlighted the preparation of M_1-N_x-C_y based SACs using the support anchoring strategy and coordination design strategy, such as physical assistance methods and wet-chemistry methods. Besides, some advanced characterization technologies for identifying single atoms were presented, such as microscopic techniques, spectroscopic techniques, DFT calculations. And then, the environmental applications such as management of harmful gases and water purification were provided. In addition, opportunities and challenges about preparation strategy, mechanism and applications were discussed. Although gratifying progress has been made in this research field, improved preparation methods, advanced characterization technologies, and diversified applications are very much needed. As this field is a research hotspot and is developing rapidly, we can only provide a temporary view in this review. However, we hope that this preliminary discussion will arouse the interest of scholars in the fields of materials, energy, environment, *etc*., and therefore expand the scope of future applications of SACs.

Declaration of competing interest

The authors declare that they have no known competing financial interests or personal relationships that could have appeared to influence the work reported in this paper.

Acknowledgments

This work was partially supported by the National Natural Science Foundation of China (No. 51979294), the U.S. Department of Agriculture (No. 2018-68011-28371) and the National Science Foundation (No. 1833988), the Training Program for Excellent Young Innovators of Changsha (No. kq1905064).

References

[1] S. De, J. Zhang, R. Luque, N. Yan, Energy Environ. Sci. 9 (2016) 3314–3347.
[2] J. Zhang, Z. Xia, L. Dai, Sci. Adv. 1 (2015) e1500564.
[3] W. Zang, Z. Kou, S.J. Pennycook, J. Wang, Adv. Energy Mater. 10 (2020) 1903181.
[4] H. Zhang, G. Liu, L. Shi, J. Ye, Adv. Energy Mater. 8 (2018) 1701343.
[5] A. Wang, J. Li, T. Zhang, Nat. Rev. Chem. 2 (2018) 65–81.
[6] X. Cui, W. Li, P. Ryabchuk, et al., Nat. Catal. 1 (2018) 385–397.
[7] B. Qiao, A. Wang, X. Yang, et al., Nat. Chem. 3 (2011) 634–641.
[8] H. Yan, C. Su, J. He, W. Chen, J. Mater. Chem. A 6 (2018) 8793–8814.
[9] L. Wang, M.X. Chen, Q.Q. Yan, et al., Sci. Adv. 5 (2019) eaax6322.
[10] P. Liu, Y. Zhao, R. Qin, et al., Science 352 (2016) 797–800.
[11] C. Paolucci, I. Khurana, A.A. Parekh, et al., Science 357 (2017) 898–903.
[12] X. Li, X. Huang, S. Xi, et al., J. Am. Chem. Soc. 140 (2018) 12469–12475.
[13] J. Shan, M. Li, L.F. Allard, et al., Nature 551 (2017) 605–608.
[14] L. Nie, D. Mei, H. Xiong, et al., Science 358 (2017) 1419–1423.
[15] K. Kim, T. Lee, Y. Kwon, et al., Nature 535 (2016) 131–135.
[16] M. Liu, N. Li, S.F. Cao, et al., Adv. Mater. 34 (2022) 2107421.
[17] Y. Zhu, W. Peng, Y. Li, et al., Small Methods 3 (2019) 1800438.
[18] W.H. Lai, Z. Miao, Y.X. Wang, et al., Adv. Energy Mater. 9 (2019) 1900722.
[19] V. Muravev, G. Spezzati, Y.Q. Su, et al., Nat. Catal. 4 (2021) 469–478.
[20] H.J. Wang, L. Jiao, L.R. Zheng, et al., Adv. Funct. Mater. 31 (2021) 2103465.
[21] R.T. Hannagan, G. Giannakakis, R. Reocreux, et al., Science 372 (2021) 1444.
[22] E. Jung, H. Shin, B.H. Lee, et al., Nat. Mater. 19 (2020) 436–442.
[23] X. Wan, X. Liu, Y. Li, et al., Nat. Catal. 2 (2019) 259–268.
[24] L. Jiao, H.L. Jiang, Chem 5 (2019) 786–804.
[25] K. Maiti, S. Maiti, M.T. Curnan, et al., Adv. Energy Mater. 11 (2021) 2101670.
[26] Y. Shang, X. Xu, B. Gao, et al., Chem. Soc. Rev. 50 (2021) 5281–5322.
[27] A. Han, B. Wang, A. Kumar, et al., Small Methods 3 (2019) 1800471.
[28] X. Huang, H. Yan, L. Huang, et al., J. Phys. Chem. C 123 (2018) 7922–7930.
[29] X. Cui, J. Xiao, Y. Wu, et al., Angew. Chem. Int. Ed. 55 (2016) 6708–6712.
[30] D. Deng, X. Chen, L. Yu, et al., Sci. Adv. 1 (2015) e1500462.
[31] H.L. Wang, X. Wang, J. Pan, et al., Angew. Chem. Int. Ed. 60 (2021) 23154–23158.
[32] L. Cao, Q. Luo, J. Chen, et al., Nat. Commun. 10 (2019) 4849.
[33] L. Cao, Q. Luo, W. Liu, et al., Nat. Catal. 2 (2019) 134–141.
[34] X. Hai, S.B. Xi, S. Mitchell, et al., Nat. Nanotechnol. 17 (2022) 174–178.
[35] H. Yang, Q. Lin, C. Zhang, et al., Nat. Commun. 11 (2020) 593.
[36] Y. Zhao, J. Liang, C. Wang, et al., Adv. Energy Mater. 8 (2018) 1702524.
[37] W. Liu, L. Zhang, X. Liu, et al., J. Am. Chem. Soc. 139 (2017) 10790–10798.
[38] H. Zhang, Y. Liu, T. Chen, et al., Adv. Mater. 31 (2019) e1904548.
[39] P. Zhou, L. Jiang, F. Wang, et al., Sci. Adv. 3 (2017) e1601945.
[40] Y.X. Li, S.L. Zhang, W.R. Cheng, et al., Adv. Mater. 34 (2022) 2105204.
[41] N. Cheng, S. Stambula, D. Wang, et al., Nat. Commun. 7 (2016) 13638.
[42] K. Yamazaki, Y. Maehara, R. Kitajima, et al., Appl. Phys. Express 11 (2018) 095101.
[43] Z. Chen, E. Vorobyeva, S. Mitchell, et al., Nat. Nanotechnol. 13 (2018) 702–707.
[44] H. Fei, J. Dong, C. Wan, et al., Adv. Mater. 30 (2018) e1802146.

[45] Y. Yao, Z. Huang, P. Xie, et al., Nat. Nanotechnol. 14 (2019) 851–857.
[46] Y. Qu, Z. Li, W. Chen, et al., Nat. Catal. 1 (2018) 781–786.
[47] Z. Yang, B. Chen, W. Chen, et al., Nat. Commun. 10 (2019) 3734.
[48] T. Li, J. Liu, Y. Song, F. Wang, ACS Catal. 8 (2018) 8450–8458.
[49] H. Wei, H. Wu, K. Huang, et al., Chem. Sci. 10 (2019) 2830–2836.
[50] X. Cui, H. Li, Y. Wang, et al., Chem 4 (2018) 1902–1910.
[51] L. Bai, C.S. Hsu, D.T.L. Alexander, et al., J. Am. Chem. Soc. 141 (2019) 14190–14199.
[52] L. Zhang, L. Han, H. Liu, et al., Angew. Chem. Int. Ed. 56 (2017) 13694–13698.
[53] P. Huang, J. Huang, S.A. Pantovich, et al., J. Am. Chem. Soc. 140 (2018) 16042–16047.
[54] F. Li, G.F. Han, H.J. Noh, et al., Energy Environ. Sci. 11 (2018) 2263–2269.
[55] L. Liu, X. Wu, L. Wang, et al., Commun. Chem. 2 (2019) 18.
[56] H. Fei, J. Dong, Y. Feng, et al., Nat. Catal. 1 (2018) 63–72.
[57] L. Liu, H. Su, F. Tang, et al., Nano Energy 46 (2018) 110–116.
[58] P. Meng, A. Brock, Y. Xu, et al., J. Am. Chem. Soc. 142 (2020) 479–486.
[59] L. Yang, D. Cheng, H. Xu, et al., PNAS 115 (2018) 6626–6631.
[60] L. Yang, L. Shi, D. Wang, et al., Nano Energy 50 (2018) 691–698.
[61] W. Zang, T. Yang, H. Zou, et al., ACS Catal. 9 (2019) 10166–10173.
[62] P. Zhou, N. Li, Y. Chao, et al., Angew. Chem. Int. Ed. 58 (2019) 14184–14188.
[63] Y. Zhu, W. Sun, J. Luo, et al., Nat. Commun. 9 (2018) 3861.
[64] M. Zhang, Y.G. Wang, W. Chen, et al., J. Am. Chem. Soc. 139 (2017) 10976–10979.
[65] A. Alarawi, V. Ramalingam, J.H. He, Mater. Today Energy 11 (2019) 1–23.
[66] S.M. George, Chem. Rev. 110 (2010) 111–131.
[67] S. Wang, P. Zhou, L. Zhou, et al., Nano Lett. 21 (2021) 4262–4269.
[68] I. Bilecka, M. Niederberger, Nanoscale 2 (2010) 1358–1374.
[69] X. Xu, X. Zhang, Z. Xia, et al., J. Energy Chem. 54 (2021) 579–586.
[70] H. Wei, K. Huang, D. Wang, et al., Nat. Commun. 8 (2017) 1490.
[71] X.W.H. Wang, J. Pan, L. Zhang, et al., Angew. Chem. Int. Ed. 60 (2021) 23154–23158.
[72] L.C. Bai, C.S. Hsu, D.T.L. Alexander, et al., Nat. Energy 6 (2021) 1054–1066.
[73] J. Liu, B.R. Bunes, L. Zang, C. Wang, Environ.Chem. Lett. 16 (2018) 477–505.
[74] X. Zhu, D. Zhang, C.J. Chen, et al., Nano Energy 71 (2020) 104597.
[75] D.A. Bulushev, A.D. Nishchakova, S.V. Trubina, et al., J. Catal. 402 (2021) 264–274.
[76] G.C. Huang, Q. Niu, J.W. Zhang, et al., Chem. Eng. J. 427 (2022) 131018.
[77] X. Wang, J. Du, Q. Zhang, et al., Carbon 157 (2020) 614–621.
[78] M. Zhang, Y. Wang, W. Chen, et al., J. Am. Chem. Soc. 139 (2017) 10976–10979.
[79] P. Peng, L. Shi, F. Huo, et al., Sci. Adv. 5 (2019) eaaw2322.
[80] L. Zhao, Y. Zhang, L.B. Huang, et al., Nat. Commun. 10 (2019) 1278.
[81] X. He, Q. He, Y. Deng, et al., Nat. Commun. 10 (2019) 3663.
[82] M. Xiao, J. Zhu, G. Li, et al., Angew. Chem. Int. Ed. 58 (2019) 9640–9645.
[83] F. Lü, S. Zhao, R. Guo, et al., Nano Energy 61 (2019) 420–427.
[84] S. Chen, W.H. Li, W. Jiang, et al., Angew. Chem. Int. Ed. 61 (2022) e202114450.
[85] J. Gu, C.S. Hsu, L. Bai, et al., Science 364 (2019) 1091–1094.
[86] F. Pan, H. Zhang, K. Liu, et al., ACS Catal. 8 (2018) 3116–3122.
[87] Y. Wang, J. Mao, X. Meng, et al., Chem. Rev. 119 (2019) 1806–1854.
[88] J. Guo, J. Huo, Y. Liu, et al., Small Methods 3 (2019) 1900159.
[89] Q. Liu, Z. Zhang, Catal. Sci. Technol. 9 (2019) 4821–4834.
[90] Z.H. Lin, Q.R. Zhang, J. Pan, et al., Energy Environ. Sci. 15 (2022) 1172–1182.
[91] H. Wu, H. Li, X. Zhao, et al., Energy Environ. Sci. 9 (2016) 3736–3745.
[92] J. Wu, L. Xiong, B. Zhao, et al., Small Methods 4 (2019) 1900540.
[93] X. Wei, D. Zheng, M. Zhao, et al., Angew. Chem. Int. Ed. 59 (2020) 14639–14646.
[94] Z.P. Miao, X.M. Wang, Z.L. Zhao, et al., Adv. Mater. 33 (2021) 2006613.
[95] K.C. Kwon, J.M. Suh, R.S. Varma, et al., Small Methods 3 (2019) 1800492.
[96] P. Yin, T. Yao, Y. Wu, et al., Angew. Chem. Int. Ed. 55 (2016) 10800–10805.
[97] H. Cao, G.J. Xia, J.W. Chen, et al., J. Phys. Chem. C 124 (2020) 7287–7294.
[98] Y. Zhou, W. Yang, W. Utetiwabo, et al., J. Phys. Chem. Lett. 11 (2020) 1404–1410.
[99] Z.J. Li, W. Wei, H.H. Li, et al., ACS Nano 15 (2021) 10175–10184.
[100] M. Hu, S. Li, S. Zheng, et al., J. Phys. Chem. C 124 (2020) 13168–13176.
[101] Y.T. He, X.X. Yang, Y.S. Li, et al., ACS Catal. 12 (2022) 1216–1227.
[102] G. Zhu, F. Liu, Y. Wang, et al., Phys. Chem. Chem. Phys. 21 (2019) 12826–12836.
[103] M.D. Esrafili, B. Nejadebrahimi, Appl. Surf. Sci. 475 (2019) 363–371.
[104] H. Zhang, P. An, W. Zhou, et al., Sci. Adv. 4 (2018) eaao6657.
[105] Y. Shang, X. Duan, S. Wang, et al., Chin. Chem. Lett. 33 (2022) 663–673.
[106] H. Zhang, L. Peng, A. Chen, et al., Carbohydr. Polym. 214 (2019) 276–285.
[107] X. Hu, W. Wang, G. Xie, et al., Chemosphere 216 (2019) 733–741.
[108] G. Xie, H. Wang, Y. Zhou, et al., J. Taiwan Inst. Chem. E 112 (2020) 357365.
[109] M. Huang, Y. Li, M. Li, et al., Environ. Sci. Technol. 53 (2019) 3610–3619.
[110] H.A. Bicalho, J.L. Lopez, I. Binatti, et al., Mol. Catal. 435 (2017) 156–165.
[111] R. Trofimovaite, C.M.A. Parlett, S. Kumar, et al., Appl. Catal. B: Environ. 232 (2018) 501–511.
[112] Q. Shen, C. Cao, R. Huang, et al., Angew. Chem. Int. Ed. 59 (2020) 1216–1219.
[113] X. Ge, P. Zhou, Q. Zhang, et al., Angew. Chem. Int. Ed. 59 (2019) 232–236.
[114] D. Xia, H. Liu, B. Xu, et al., Appl. Catal. B: Environ. 245 (2019) 177–189.
[115] Y. Tang, W. Chen, Z. Shen, et al., Carbon 111 (2017) 448–458.
[116] S. Wang, J. Li, Q. Li, et al., Nanoscale 12 (2020) 364–371.
[117] Z. Wang, J. Zhao, J. Wang, et al., J. Mater. Chem. A 6 (2018) 7547–7556.
[118] G. Lei, W. Zhao, L. Shen, et al., Appl. Catal. B: Environ. 267 (2020) 118663.
[119] G.M. Liu, Y. Huang, H.Q. Lv, et al., Appl. Catal. B: Environ. 284 (2021) 119683.
[120] S. An, G. Zhang, T. Wang, et al., ACS Nano 12 (2018) 9441–9450.
[121] M. Chen, N. Wang, L. Zhu, Catal. Today 348 (2020) 187–193.
[122] J. Gao, Y. Wang, S. Zhou, et al., ChemCatChem 9 (2017) 1708–1715.
[123] Y. Wang, X. Zhao, D. Cao, et al., Appl. Catal. B: Environ. 211 (2017) 79–88.
[124] M. Pan, J. Wang, G. Gao, J.W. Chew, J. Membr. Sci. 602 (2020) 117966.
[125] J.J. Liu, H. He, Z.R. Shen, et al., J. Hazard. Mater. 429 (2022) 128398.
[126] G. Lei, H. Pan, H. Mei, et al., Chem. Soc. Rev. 51 (2022) 7260–7280.
[127] T. Cui, L. Li, C. Ye, et al., Adv. Funct. Mater. 32 (2021) 2108381.
[128] Y. Tang, H. Zhang, W. Chen, et al., Appl. Surf. Sci. 508 (2020) 145245.
[129] X. Liu, Z. Gao, H. Huang, et al., Mol. Catal. 488 (2020) 110901.
[130] Y. Tang, W. Chen, B. Wu, et al., ChemPhysChem 20 (2019) 2506–2517.
[131] G.C. Lei, Y.W. Tong, L.J. Shen, et al., Small 17 (2021) 2104939.
[132] A. Beniya, S. Higashi, Nat. Catal. 2 (2019) 590–602.
[133] X. He, B.G. Looker, K.T. Dinh, et al., ACS Catal. 10 (2020) 7820–7825.
[134] S. Khan, A. Wasfi, M. Mushtaq, et al., Appl. Surf. Sci. 599 (2022) 154037.
[135] M. Flytzani-Stephanopoulos, M. Sakbodin, Z. Wang, Science 312 (2006) 1508–1510.
[136] K. Vikrant, K.H. Kim, A. Deep, Appl. Catalysis. B: Environ. 259 (2019) 118025.
[137] Y. Li, T. Yang, S. Qiu, et al., Chem. Eng. J. 389 (2020) 124382.
[138] F. Chen, X.L. Wu, L. Yang, et al., Chem. Eng. J. 394 (2020) 124904.
[139] X.M. Peng, J.Q. Wu, Z.L. Zhao, et al., Chem. Eng. J. 429 (2022) 132245.
[140] F. Wang, Y. Wang, Y. Feng, et al., Appl. Catal. B: Environ. 221 (2018) 510–520.
[141] C. Jin, J. Kang, Z. Li, et al., Appl. Surf. Sci. 514 (2020) 146076.
[142] S. Mao, C. Liu, Y. Wu, et al., Chemosphere 291 (2022) 133039.
[143] S.J. Huang, B. Hu, S.R. Zhao, et al., Chem. Eng. J. 430 (2022) 132933.
[144] X.J. Yang, X.M. Xu, J. Xu, Y.F. Han, J. Am. Chem. Soc. 135 (2013) 16058–16061.
[145] L. Chen, J. Ma, X. Li, et al., Environ. Sci. Technol. 45 (2011) 3925–3930.
[146] X.Y. Xu, F. Zhan, J.Q. Pan, et al., Chemosphere 294 (2022) 133735.
[147] J.R. Yang, P. Li, X.G. Duan, et al., J. Hazard. Mater. 430 (2022) 128463.
[148] Y. Shang, X. Liu, Y. Li, et al., Chem. Eng. J. 446 (2022) 132245.
[149] M. Yang, Z. Hou, X. Zhang, et al., Environ. Sci. Technol. 56 (2022) 11635–11645.
[150] B. Li, X. Cheng, R. Zou, et al., Appl. Catal. B: Environ. 304 (2022) 121009.
[151] X. Wang, X. Pu, Y. Yuan, et al., Chin. Chem. Lett. 31 (2020) 2634–2640.
[152] X. Liang, D. Wang, Z. Zhao, et al., Adv. Funct. Mater. 32 (2022) 2203001.
[153] A. Cabrera-Reina, A.B. Martinez-Piernas, Y. Bertakis, et al., Water Res. 166 (2019) 115037.
[154] X. Wang, X. Wang, J. Zhao, et al., Appl. Catal. B: Environ. 206 (2017) 479–489.
[155] W. Luo, L. Zhu, N. Wang, et al., Environ. Sci. Technol. 44 (2010) 1786–1791.
[156] B.J. Trześniewski, I.A. Digdaya, T. Nagaki, et al., Energy Environ. Sci. 10 (2017) 1517.
[157] G. Capilli, M. Costamagna, F. Sordello, C. Minero, Appl. Catal. B: Environ. 242 (2019) 121–131.
[158] J. Liu, H. He, Z. Shen, et al., J. Hazard. Mater. 429 (2022) 128398.
[159] P. Cui, C. Liu, X. Su, et al., Environ. Sci. Technol. 56 (2022) 8034–8042.
[160] Z. Xiong, B. Lai, P. Yang, Water Res. 140 (2018) 12–23.